Copyright 1998 by the Society of Photo-Optical Instrumentation Engineers.

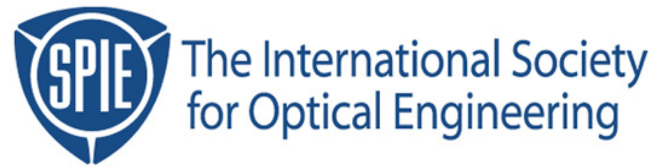

This paper was published in the proceedings of the
18th Annual BACUS Symposium on Photomask Technology and Management
SPIE Vol. 3546, pp. 288-303.
It is made available as an electronic reprint with permission of SPIE.

One print or electronic copy may be made for personal use only. Systematic or multiple reproduction, distribution to multiple locations via electronic or other means, duplication of any material in this paper for a fee or for commercial purposes, or modification of the content of the paper are prohibited.

Assessment of a Hypothetical Roadmap that Extends Optical Lithography Through the 70nm Technology Node

John S. Petersen[1], Martin McCallum[2A], Nishrin Kachwala[2B], Robert J. Socha[3],
J. Fung Chen[4], Tom Laidig[4], Bruce W. Smith[5], Ron Gordon[6], Chris A. Mack[6]

1. Petersen Advanced Lithography, PO Box 162712, Austin, TX 78716 USA
2. International SEMATECH, B. SEMATECH, 2706 Montopolis Drive, Austin, TX 78741-6499 USA
3. National Semiconductor Corp., MS E-100, 2900 Semiconductor Drive, Santa Clara, CA 95052-8090 USA
4. MicroUnity Systems Engineering, Inc. 475 Potero Avenue, Sunnyvale, CA 94086-4118 USA
5. Rochester Institute of Technology, 82 Lomb Memorial Drive, Rochester, NY 14623-5604 USA
6. FINLE Technologies, PO Box 162712, Austin, TX 78716 USA

Email 1: jpetersen@advlitho.com

Abstract

This work discusses routes to extend optical lithography to the 70 nm technology node using proper selection of masks, mask design including choice of optical proximity correction (OPC), exposure tool, illuminator design, and resist design to do imaging process integration. The goal of this integration is to make each component of the imaging system work to the best benefit of the other imaging components so as to produce focus-exposure process windows large enough to use in a manufacturing environment. In order to maximize return on investment, the design of the photoresist and the exposure tool is used to simplify reticle design as much as possible. For masks, the choices of binary, alternating or attenuated phase-shift masks (PSM) are discussed. Alternating PSM produces the best image quality but the effective phase angle depends on NA, wavelength, sigma, magnification, pitch and duty cycle. Attenuated PSM has maximum image quality when using transmissions of 18% for contact holes and 30% to 40% for lines and spaces. Using high transmission masks increases working resolution of a wide range of feature sizes and shapes, but requires suppression of unwanted light. This suppression requires using ternary attenuated PSM and in many instances necessitates critical formation of a second layer on the mask that has both the proper size and placement of the second level features. For OPC, the use of scattering bar, sub-resolution assist features to make isolated lines mimic dense exposure-focus response is discussed. For illuminators, properly tuned weak off-axis illumination is used with binary and attenuated PSM to flatten image CD while maintaining image quality at an acceptable level for the resist. For resists, the need to balance resist bias and side-lobe printing is discussed. A "work-in-progress" integration experiment is reviewed for 525 nm and 1050 nm pitches with 175 nm targeted line features imaged with a 0.53 NA, 248 nm stepper that has been modified with weak and strong off-axis illuminators and a binary reticle. Results show weak illumination produces a common process corridor for the two pitches that will need enhancement using OPC, but that the individual windows have acceptable imaging capability. Predictions of production resolution that are inferred by our simulation and experimental results are made and recommendations are given to make these predictions a reality. Based on our work we believe that, except for dense contact holes, 248 nm has the potential to be used through the 130 nm technology node and 193 nm can be used through the 100 nm node and the beginning of the 70 nm technology node. Dense contact holes will require a next generation lithography technology.

Keywords: optical lithography, phase shift mask, alternating PSM, attenuated PSM, photoresist, weak illumination, optical proximity correction, off-axis illumination, photoresist, 248 nm, 193 nm

1. Introduction

By providing the means to create temporary masks of the fine images that form the complex patterns of integrated circuits, optical lithography has fueled the explosion of the electronic revolution. But how much longer will this hold true? The Semiconductor Industry Association's (SIA) 1997 National Technology Roadmap for attaining next generation semiconductor chips predicts optical lithography will resolve the ever shrinking features of these devices until the 130 nm technology node, where a technology node is named for the highest frequency features plus the next three design shrinks. This roadmap shows both 248 nm and 193 nm lithography producing the critical images for 180 nm technology node and 193 nm lithography for the 150 nm node. Then starting at the 130 nm node, non-optical lithographic solutions are said to be required. The assumptions inherent in this roadmap are

only valid when working within an optical imaging infrastructure that is not optimally integrated. With concerns about the timely introduction of 193 nm and non-optical lithography into production, optical imaging as the next generation lithography is beginning to look more acceptable. It is now generally felt that 248 nm will work through the 150 nm node, and our work suggests that, except for dense contacts, 248 nm lithography will carry us through the 130 nm node. Then 193 nm will be used through the 100 nm technology node and possibly below.

Historically, the device design, layout, exposure tool, mask, and imageable masking material (photoresist) communities did not team to make the best possible resolution that they could. Our work shows that with proper integration of the entire imaging process, optical lithography has the potential to work clear through the 100 nm technology node to the very brink of the 70 nm node.

In early 1997, as part of a risk management strategy to provide backup to next generation lithography (NGL) technologies and to also help understand their insertion point into the SIA roadmap[1], SEMATECH started "Project DELPHI". "DELPHI" is an acronym for **D**etermining the **L**imits of **PH**otol**I**thography. As the project name implies, DELPHI explores and appraises optical imaging technologies that could be used in the production environment to extend resolution; it also looks for implementation barriers and suggests solutions. Certainly, high-resolution resist images can be made. Figure 1 shows 100 nm 1:2 line/spaces imaged with a 0.53 NA, 248 nm stepper, and 80 nm 1:2 line/spaces imaged with a 0.6NA, 193 nm stepper. But can this be achieved in production, and if so, what form will it take?

From the onset of DELPHI, maximization of the common focus-exposure process windows for all feature sizes and pitches of interest was considered paramount. To do this in production, the entire imaging process, the design and layout of the circuit with optical proximity correction (OPC), the exposure tool and the recording material (the photoresist and substrate), would be integrated to attain optimum performance. Wong et al.[2] described similar methodologies for building 1 GB DRAM using level specific image optimization. We concur that specification is required; and only differ in our pursuit of a more dynamic, level-specific optimization of the mask, OPC, illumination and resist designs used for imaging process integration[3].

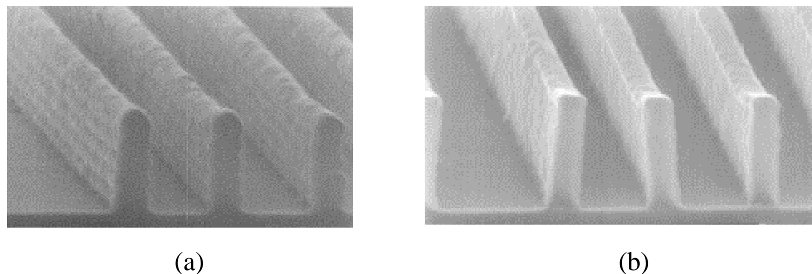

(a) (b)

Figure 1: Sample high resolution resist images using (a) 248 nm light to image 1:2 100nm features, and (b) 193 nm light to image 1:2 80 nm features.

In this work, we attempt to maximize return on investment by using the design of the photoresist and the exposure tool to simplify the reticle design as much as possible. In section 2, we discuss the mask, choice of OPC, illuminator and resist design for imaging process integration. Section 3 discusses a "work-in-progress" integration experiment. Then the final section discusses the predictions of production resolution that are inferred by our simulation[4] and experimental results, and then finishes with what we believe the integrated optical imaging community must do to make these predictions a reality.

2. Imaging Process Integration

For conventional lithography, printing smaller and smaller features involves increasing the exposure tool's numerical aperture and reducing the exposing wavelength of light. But these solutions have always had a finite normalized resolution, k_1 = feature size X NA/wavelength, of greater than 0.45. Using optical proximity correction for image shaping, resolution can be reduced to the neighborhood of k_1 = 0.4, but probably not much further for

dense 1:1 lines and spaces. Four pathways to higher resolution exist. One involves the use of strong phase shifting with conventional illumination[5]. Another uses weak phase shifting[6] with either conventional or off-axis illumination[7]. A third option uses binary mask with pupil filtering[8,9,10] and a fourth, non-phase shifting with extreme off-axis illumination to do interference imaging lithography (IIL)[11]. Pupil filtering holds promise but current exposure tools are not configured appropriately. Conceptually, IIL holds great promise but is not currently a DELPHI option, so we limited this study to the first two enhancement techniques.

These techniques involve the use of advanced photoresists, optical proximity correction, off-axis illumination, phase-shift masks and device layout that are compatible with each imaging system. On their own, these methods provide the means to image features that are smaller than the wavelength of the exposing light; so it stands to reason that optimization using an integrated approach to imaging can allow for further gains in robust, production worthy resolution. This concept of *image process integration, IPI,* of the a fore mentioned techniques to design an *integrated imaging system* will allow the manufacture of logic and memory devices that were not thought previously manufacturable with optical lithography.

2.1 Masks and Layout

In all cases we examined the use of biasing and sub-resolution assist feature OPC both in combination and separately, with the goal to use only the minimum amount needed. Of particular importance are scattering bar sub-resolution features that are small features, roughly sized at one third the exposing wavelength and placed a prescribed distance from the primary feature. These features introduce an isofocal region to an isolated line so that the image through focus behaves like a dense line, provides OPC, and reduces the Mask Error Enhancement Factor (MEEF)[12] to varying degrees, depending on the application.[13]

Figure 2 demonstrates the effect that adding scattering bars has on fairly isolated lines. This figure shows, for a 175 nm line on a 1050 nm pitch, the line's image size dependence to changes in focus at different aerial image intensities. Except for the center, each graph represents a different scattering bar distance from the primary feature, x, and the distance between scattering bars, y. The center graph has no scattering bars. Typically, k_1 of 0.6 to 0.7 spacing between primary and assist feature makes the best dense line affect. In Figure 2 this is shown in the bottom row of graphs where x equals 280 nm and 290 nm. These graphs show conjugate points for both values of x at around 240 nm to 250 nm; whereas in the top row the conjugate is near 340 nm for x equal to 180 nm, and 260 nm to 270 nm for x equal to 220 nm. The larger values of x yield a smaller size at the conjugate. Moving the conjugate towards the 175 nm target increases depth of focus. In the cases shown in Figure 2, x equal to 280 nm and 290 nm have an 800 nm depth of focus at the 200 nm aerial image size. This is the size that approximately corresponds to the intensity threshold that is sampled by the resist before shrinking to the resist image size of 175 nm after post-exposure bake and development. This depth of focus is twice as good as that for x equal to 180 nm and 220 nm, and four times better than having no assist features at all. However, for these large values of x, y is less than the wavelength and, under certain conditions, the two scattering bars may print as a single line. Lowering the image quality and raising the intensity of the scattering bar by half-toning the assist features (breaking the solid lines into dots) or by making the scattering bar line smaller eliminates the danger of printing. Other methods to prevent printing of the assist features will be discussed in the resist section 2.3.

Finally, until recently the size of the scattering bar lines, while not critical[12], were difficult for the mask maker to fabricate with current technology[14]. The difficulty arose from the need to have a linear resolution of 240 nm on the mask, increased data handling, and lower fabrication process bias. Recent evidence from MicroUnity shows that with increased demand the assist feature fabrication has improved and now leading-edge mask houses make them routinely.

For the printing of lines and spaces of k_1 equal to 0.25, the use of strong phase-shifting is by far the more powerful of the two shifting techniques. However, because of unfriendly designs, the layout causes unwanted phase-edges that must be eliminated and conditions where no layout solution is possible[15]. Also, as previously published[16,17,18,19,20], subtractive fabrication techniques give rise to aerial image imbalances between the alternating shifter regions. These imbalances give rise to image placement issues that limit depth of focus (DoF) and ultimately limit the allowed duty cycle and attainable pitch that can be imaged. Using a global or dual trench[16,19] or undercut etch[18], these images are balanced at "best focus" but change through focus, suggesting a phase-error. Figure 3 demonstrates what is observed. In this figure the center plot shows the aerial intensity of alternating phase spaces about a chrome line at the apparent center of focus. In this plot the point we call center is chosen because the

intensities to either side of the line are nearly balanced. Because of phase error as the image is defocused an imbalance in the aerial image is observed that changes as the image is defocused from one side of center to the other side. This phase error gives rise to shifts in center of focus with pitch[21], and gives rise to image placement error that causes a change in pitch size with focus[22]. Experimentally, the change in pitch size and change in center of focus is shown in Figure 3(b) for 1:1 180 nm and 140 nm lines and spaces. For these data the left pitch corresponds to the "0-shifter" space to the left of its line and right pitch contains the "π-shifter" to the right of the same line. The center of focus is –0.5 µm for the 180 nm features and –0.46 µm for the 140 nm lines. The slopes of these lines are indicative of approximately a plus ten degrees phase angle error[22]. Phase-error has NA, sigma, magnification, pitch, duty cycle, index of refraction, phase trench and dual trench depth dependencies that may not be correctable over all features[20]. Comparing slopes of pitch size through focus demonstrates phase dependence on pitch and duty with larger pitch and duty structures having less change in size.[22].

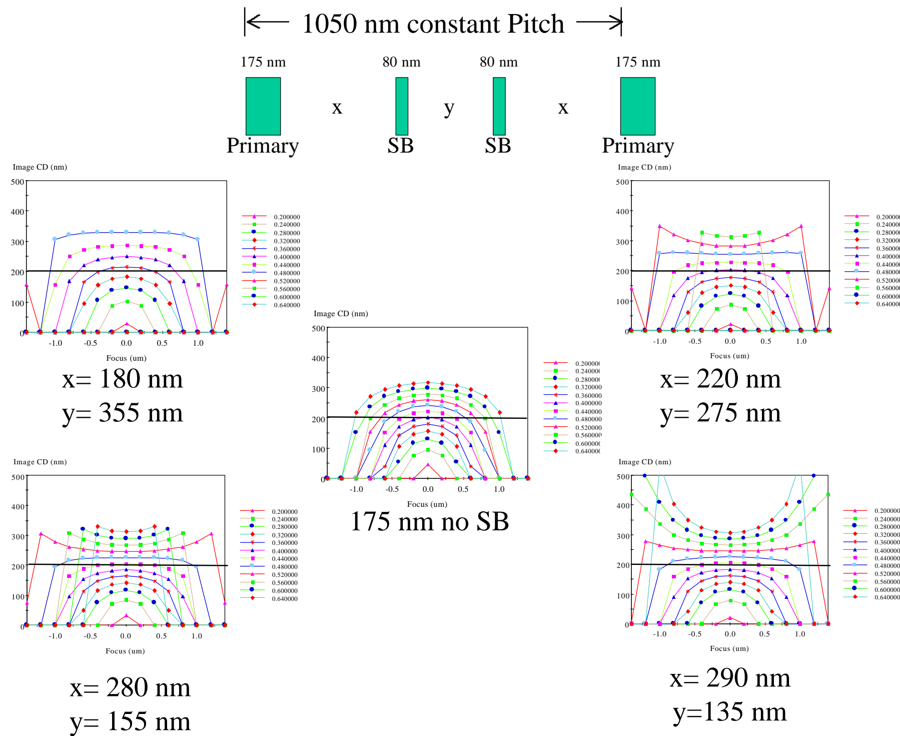

Figure 2: Aerial image size relative to changes in focus for different aerial image intensities for 175 nm line, 1050 nm pitch. Each graph represents a different scattering bar distance from the primary feature, x, and the distance between scattering bars, y. The center graph has no scattering bars. The solid line at 200 nm roughly marks the image width where the aerial image is sampled to give the final 175 nm resist image.

Regardless of the image imbalance problem, altPSM delivers impressive results. Figure 4 shows that with binary OPC a wide pitch range for 100 nm lines imaged with 248 nm, 0.53 NA is correctable[19]. Extending this to 193 nm, using an ARCH Chemical experimental bilayer resist provides a stab at the 70 nm technology node. Figure 5 shows the DoF for 40 nm-chrome lines with pitches of 180 nm, 200 nm, 220 nm and 240 nm. In this figure, DoF is 400 nm for the 50 nm resist images, 220 nm and 240 nm pitches, increasing to 500 nm DoF for the 180 nm and 200 nm pitches. Also, there is a loss in linear response across the pitch range that normally we would consider correcting with OPC as in the previous figure. It is interesting to note that for altPSM the loss of linear resolution with pitch occurs near k_{pitch} of 0.75. This is analogous to $k_1 = 0.75$ with a binary mask[23] and is a result of the placement of the first diffraction orders through the lens being in the same place for the two types of imaging. This time, however, we will use this loss of linearity as OPC to show how we can image 1:1.7 66 nm lines simultaneously with 1:3.4 and 1:3.8 50 nm lines. The ultimate limit of this 0.6 NA, 193 nm, 10X stepper should be

a 160 nm pitch, but these were not resolved because the aerial image imbalance problem caused pattern failure. Eliminating image imbalance is paramount to attaining the 70 nm node using 193 nm lithography.

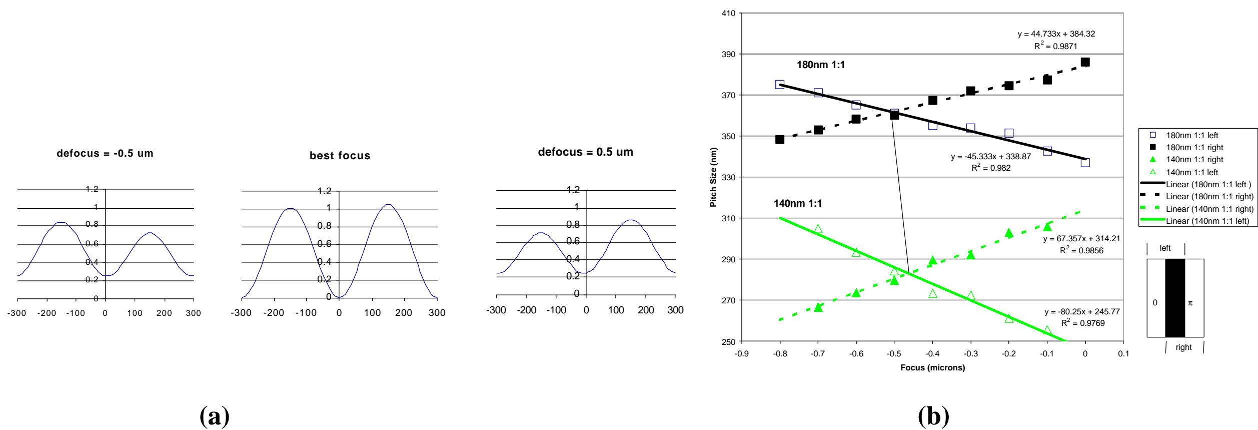

(a) **(b)**

Figure 3: AltPSM aerial image imbalance examples; (a) shows phase error induced intensity change through focus[20]; (b) pitch size dependence on focus shows evidence of both image imbalance and phase error[22].

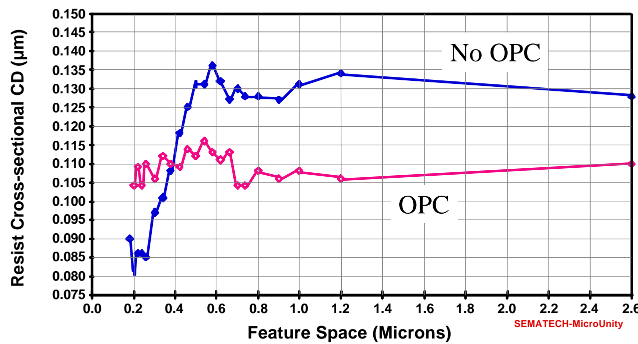

Figure 4: Resist image size for 100 nm lines relative to companion space size for AltPSM. The without OPC case has an all pitch bias of 55 nm that was reduced to 12 nm with OPC[19].

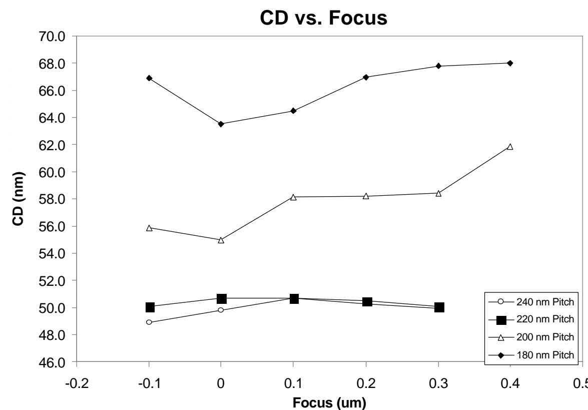

Figure 5: Depth of focus for 40 nm lines of pitch 180 nm, 200 nm, 220 nm and 240 nm. These lines were imaged with a 193 nm, 0.6 NA, 10X stepper using an experimental Olin bilayer resist. Courtesy of Olin Microelectronics Materials.

Weak shifting improves working resolution at k_1's of 0.4 and larger, but needs off-axis illumination (OAI) to extend resolution to k_1 of 0.3 to 0.37. Our work uses modified illumination as dictated by what we are trying to image. In general, we use OAI for lines and spaces and conventional illumination for contact holes. For small contacts, $k_1<0.8$, we can also use OAI, but because the intensity is already low, we did not want to throw away a diffraction term, lowering it even more. Further, contact hole layouts, with their wide range of pitches and configurations, do not generally lend themselves nicely to OAI.

One of the most common weak phase shifters is the attenuated PSM (attPSM). In particular, we are studying the use of high transmission ternary attPSM (HTTattPSM) for bright field lines and spaces. Simulation suggests that these masks appear to reduce iso-dense bias, external-internal line bias and line end shortening; thus reducing the aggressiveness of the OPC needed for the small critical features. This is shown in Figure 6. The transmission from 15% to 42% looks best for lines and spaces. Figure 7 shows the normalized image log-slope (NILS) for 175 nm lines of varying transmission (%T) and focus. NILS is the first derivative of the log(intensity of the aerial image) at the edge of the feature and it describes the image quality. On this type of reticle we use non-phase shifted sub-resolution assist features[24], as proposed by Tounai, called scattering bars. To minimize exposure of resist in dark areas of features greater than 300 nm, we use chrome shields. Presently we believe that these shields can cover 100% of the larger lines but we are also investigating attenuated rim-shifted structures so that process window overlap is insured for all features.

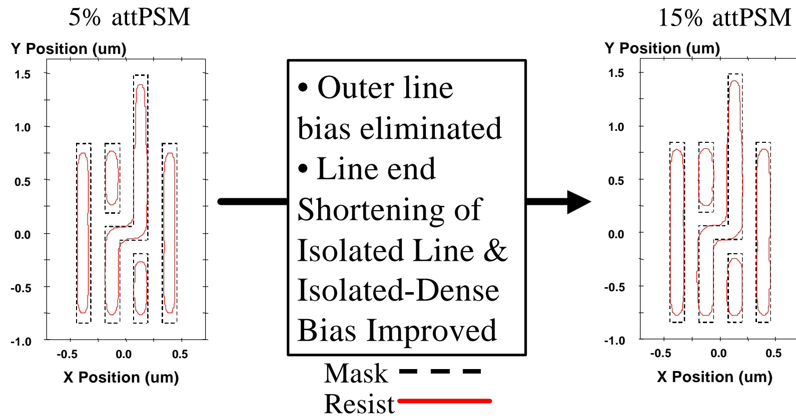

Figure 6: Simulations[4] showing the potential imaging enhancements of HTTattPSM for 130 nm features imaged with 193 nm, 0.6 NA, and weak quadrupole exposure.

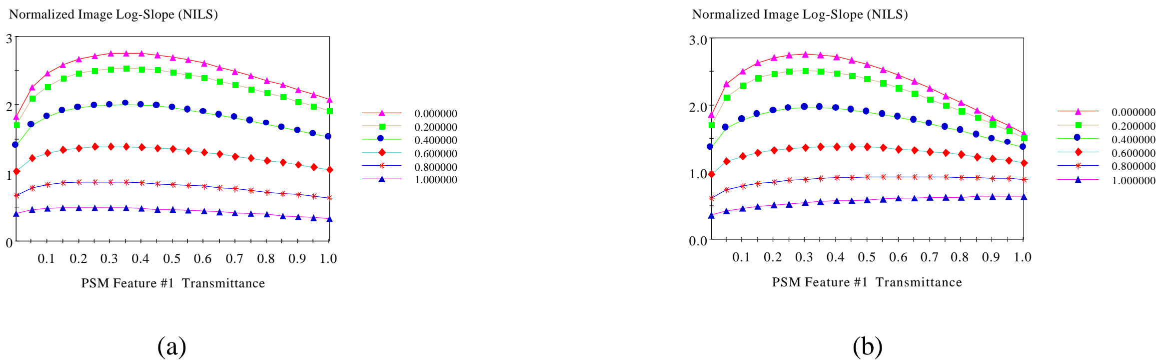

Figure 7: Normalized image log-slope for k_{pitch} = 1.12 and 2.12 calculated with 0.53 NA, 248 nm and weak quadrupole sigma center = 0.6 and sigma radius = 0.25. Plots show NILS versus attPSM %T for varying focus conditions for 175 nm features on (a) 525 nm pitch, and (b) 1050 nm pitch. Maximum NILS is found in the 15% to 45% transmission range.

For contacts, we chose to explore Bessel contacts that were first proposed by Schellenberg et al. as being the best for extending contact hole resolution and DoF[25,26]. We found that 18% is the optimum transmission for 140 nm, 170 nm and 200 nm contacts of varying pitches[27, 28]. This is also shown in Figure 8 where depth of focus versus phase is shown for attPSM %T from 2 to 24. The simulations in this figure are simple 240 nm 1:1 contacts targeted to size at 200 nm using a 248 nm, 0.63 NA, 0.3 sigma exposure.

To prevent unwanted exposure of the resist, the vias are surrounded with chrome as proposed by Ma and Andersson[29], and use sub-resolution phase edges, called antiscattering bars, and chrome scattering bars[30]. As shown in Figure 9, these OPC structures suppress the intensity of overlapping side-lobes that form naturally from the overlap of a contact's individual side-lobes with those of its nearest neighbors. This figure represents a simulation of an intensity profile for an infinite array of contacts. The intensity map on the left shows very intense side-lobes and the figure on the right shows the same array with their suppression. In our design work, we leverage the Bessel-like behavior of attPSM contacts to design our masks, choosing side-lobe suppression techniques to maintain the maximum intensity, I_{max} of the contact while maintaining a constant ratio of I_{max} to $I_{side\text{-}lobe}$. The suppression technique used is dependent on the pitch and duty cycle and where it is in the array. Contacts at the corners and sides of the array are tuned by extending the OPC to beyond the array perimeter. Experimentally, using an 18% HTTattPSM the technique has proven successful with 140 nm contacts over a pitch range of 500 nm to 1400 nm. These data show that across a 10% exposure latitude window that the 500 nm pitch contacts had a 0.6 µm DoF, and the 700 nm and 1400 nm pitches had 0.4 to 0.45 µm DoF, respectively. And by relaxing the exposure window to 5%, a DoF of 0.65 µm for the 500nm pitch and 0.55 µm for the isolated contacts was obseerved.[28]

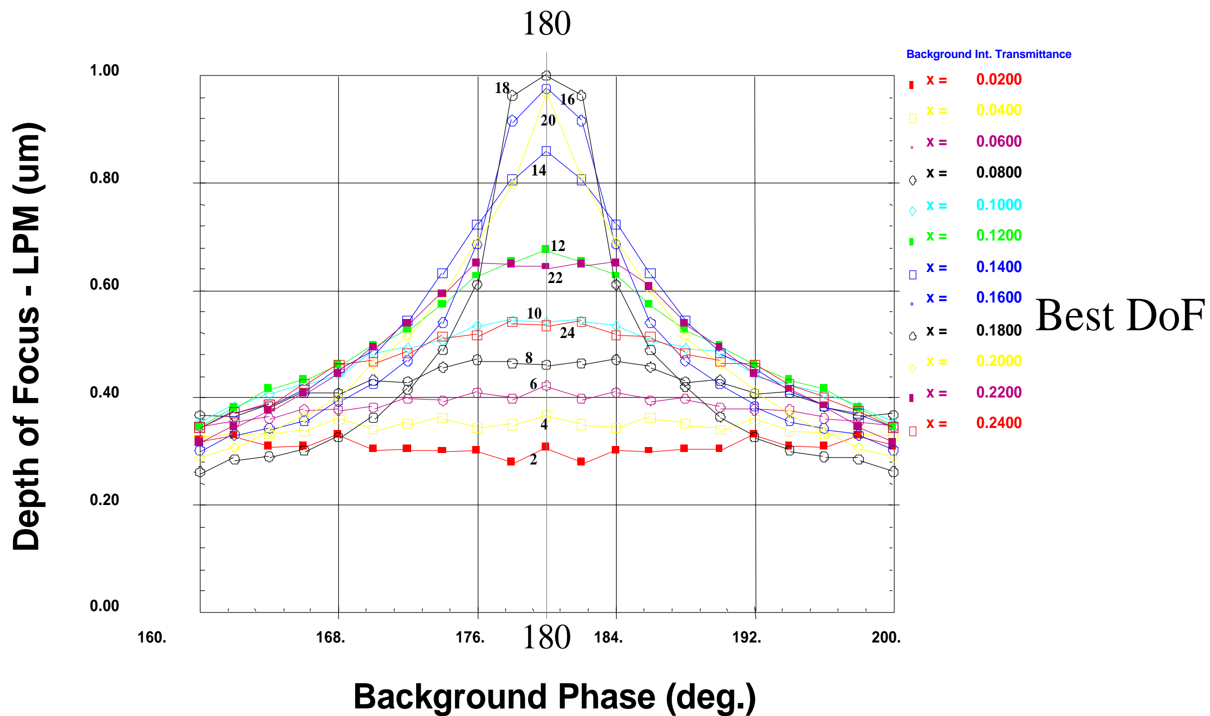

Figure 8: Lumped parameter model[4] depth of focus versus phase for attPSM transmission from 2% to 24%. Exposure parameters: 248 nm, 0.63 NA, 0.3 sigma, infinite contact hole array mask with a 480 nm pitch, 240 nm contacts and 200 nm target dimension and no side-lobe suppression.

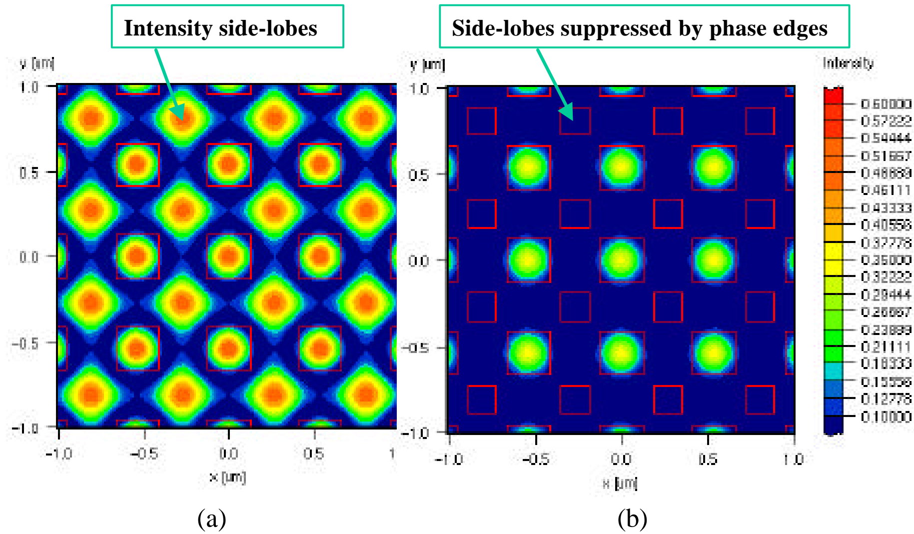

Figure 9: Simulations of contact holes using 18% attPSM. Intensity map shows (a) an uncorrected image, and (b) the same features with the side-lobes suppressed using phase edges from antiscattering bars.

In these designs the overall brightness of the contact is driven by how bright a side-lobe the resist can tolerate without printing. Referring again to Figure 9 notice that side-lobe intensity suppression reduces intensity in the contact and reduces the NILS. To enhance both, image process integration dictates development of resist processes that tolerate side-lobes. Yasuzato et al. accomplished this by soaking the resist in tetramethylammonium hydroxide, TMAH, to make a base insoluble layer in both novolak-diazonaphthoquinone I-line resist and chemically amplified positive deep UV resists[31]. Recent advances from Shipley, shown in Figure 10, have taken resists with zero side-lobe intensity tolerance to ones that do not print them within the critical focus-exposure process window. To first order, increasing the non-linear response of the resist to subthreshold exposure doses does this. The metric Shipley uses is the c-value, the ratio of the open field dose to retain 95% of the post develop thickness (E_{95}) and the minimum dose to attain zero thickness (E_0)[32]. In section 2.3, resist tuning will be revisited. It is hoped that continued improvements in resist will open the design of the contact holes and will allow for better and better imaging performance. This holds true for lines and spaces as well and is a perfect example of the need for image process integration.

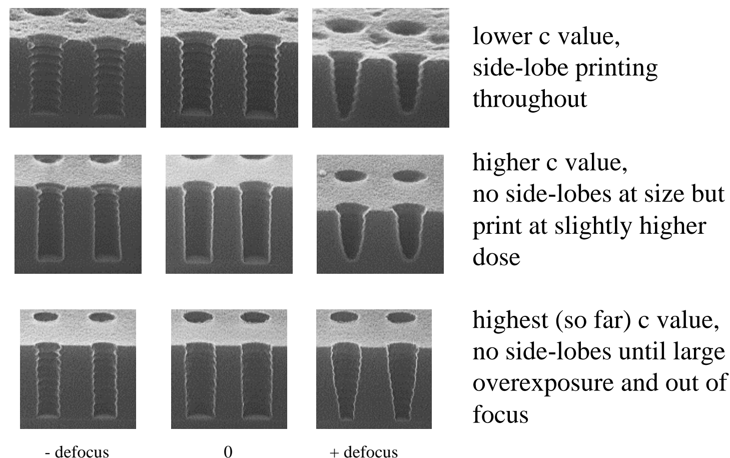

Figure 10: Resist images of three different resists, one per row, and three different focus conditions. Contacts are 200 nm on a 480 nm pitch, imaged with a 248 nm, 0.53 NA, 0.74 sigma stepper. The suppression of side-lobe printing improves from top row to bottom. Data courtesy of Shipley.

Finally, as with altPSM there are issues with fabricating attPSM and HTTattPSM. First, the dominant material used today is a bilevel attenuator made of Mo-Si-N. One level is used for controlling transmission and the other for controlling phase. As the TEM in Figure 11 shows, the different levels have different etch characteristics that give rise to different wall profiles. Also, because of similarities between the Mo-Si-N and the quartz, the quartz is attacked during the etch. Thus, this low etch selectivity makes it difficult to over-etch the attenuator to improve the sidewall profile without damaging the quartz and creating a phase error. One possible solution is to make 175 degree attenuated phase plates, so that an anisotropic over-etch into the quartz would straighten the wall profile and bring the phase to 180 degrees. However, all things being equal, the ideal situation is to use an attenuator that has better etch selectivity to quartz. Another issue is the ability to make ternary attPSM using a critical layer to layer alignment, whose placement tolerance is still being determined but will probably be less than 100 nm to target. This is possible as shown in Figure 12, but the proper alignment processes may need to be improved for day to day production of these types of reticles.

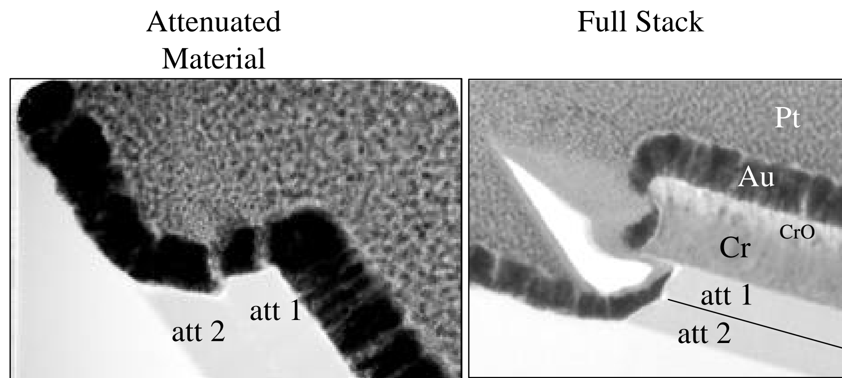

Figure 11: TEM of a typical attPSM blank showing the bilevel attenuated material.

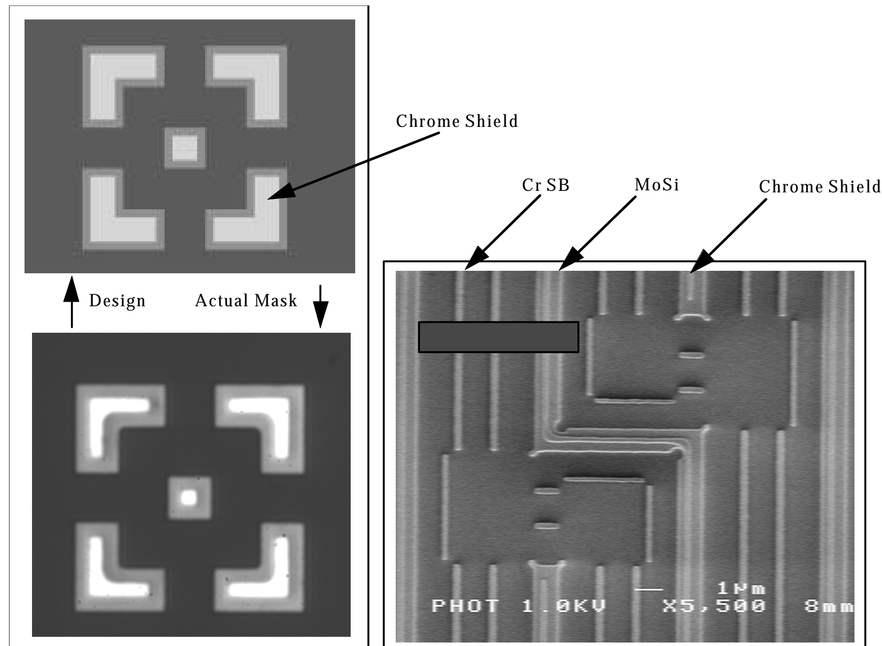

Figure 12: Overlay marks and test features for a 6% ternary attPSM shows that even with good overlay on the alignment mark there can be errors in the live feature.

2.2 Illumination

The gain from using OAI, as shown in Figure 13, is accomplished by replacing the three beam imaging of the plus first, minus first, and zero diffraction orders of conventional on-axis illumination with the two beam imaging of a single first and zero order[33,34]. OAI thus halves the cone angle and effectively doubles the acceptance angle to relay interferable beams of light to the image plane at the wafer and works best for interfering beams that are radially symmetric about the optical axis. OAI works independent the use of weak phase shifting. However, to balance the intensity of the zero and first order beams, weak phase shifting in combination with OAI has proven useful[7]. Also, although OAI with center or axial sigma very near one maintains the information transfer of small features, because of non-optimal interference the image quality (as defined by the normalized log-slope of the aerial image) is greatly reduced. Using a weak phase shifting technique improves image quality in this case[35].

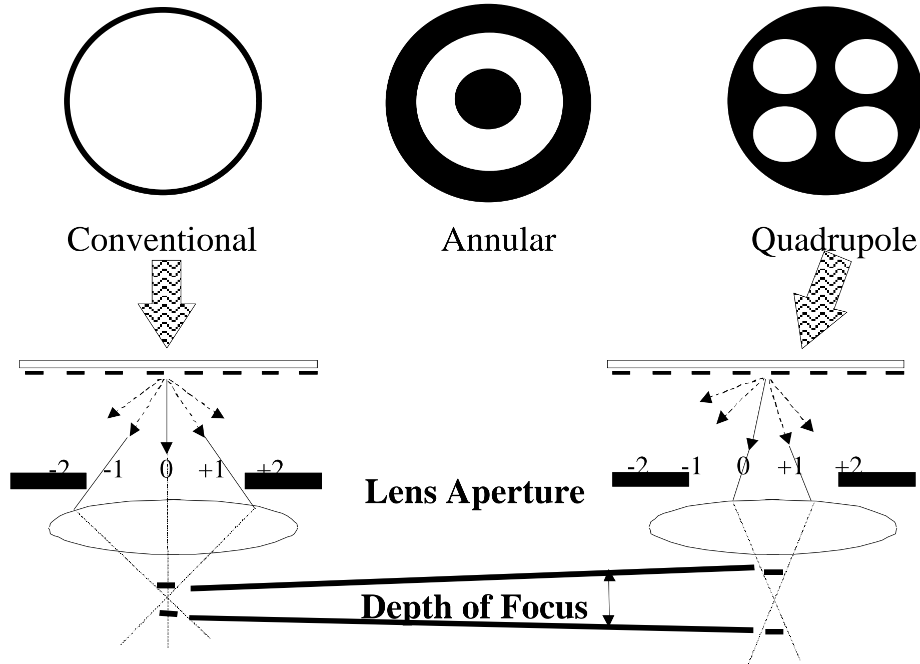

Figure 13: Comparison of on-axis and off-axis illumination.

Again referring to Figure 13, there are two general OAI shapes, annular and quadrupole, that both work essentially the same way. Primarily we use quads because they provide higher image quality for Manhattan geometries than does an annulus that tends to have a larger DC component of light. The most common quad configuration is four individual poles placed one within each quadrant of the illuminator pupil orientated on the 45° line from the optical x and y axis. Maximum two-beam interference occurs when the interfering beams are radially symmetric about the center of the optical axis and there is a minimum of non-radially symmetric interference. Ideal symmetry occurs at:

$$\sigma_{center} = \frac{\lambda}{\sqrt{2} \cdot pitch \cdot NA}$$

Where λ equals the actinic wavelength of light; NA is the numerical aperture of the projection lens; σ is the ratio of the illuminator NA to the NA of the projection lens and σ_{center} is the radial position of the pole, 45° from the x and y optical axis. The only time this occurs is if the diffraction orders are point apertures limiting each diffraction pattern to a single interference angle. These infinitesimal illuminators would yield infinite depth of focus that in practice never occurs because there is a radial component about the σ_{center} that creates a finite set of interference angles that act to degrade the image.[36] An extreme case of this degradation occurs with isolated lines, where there is no discrete

diffraction pattern and the feature is best described as a continuous sin(x)/x function. In this case, some optimal interference occurs but most is not and acts to degrade the image.[36, 37]

Giving the isolated line some dense line behavior by adding scattering bars helps improve the image quality with OAI.[37] But it is important to keep in mind that addition of the scattering bars must be done in a way to match NILS and image CD across the desired focus range and in many instances degrading the image a little with OAI might be desirable.[38], [39]

As for the quad designs, based on work by Ogawa[40], we pursued the use of weak quads, meaning light exists between the poles, and for reference compared it to strong, where there is no light between the poles. Weak quads can be designed in three different ways. The simplest is placement of the four poles with top-hat intensity distributions on the optical x-axis and y-axis, the next is to add a background transmission to a strong quad and the third is made by merging the tails of four Gaussian shaped poles[35]. The correct Gaussian as defined by the radial sigma at half height and distance from the optical center to the center of the Gaussian, the center sigma, defines the width and contrast of the critical features and pitches. The goal in weak quad design is to minimize the need for OPC by flattening the image CD and the NILS within a feature size for all the pitches of interest while at the same time maintaining image quality at a level at which the resist can adequately respond.[35,]

2.3 Resist and Image Process Integration

Photoresists sample the latent image in the resist along dose contours that range from some threshold value to the lowest dose found in the image. The degree of the response is related to the quality of the projected image that forms in the resist and where the resist samples the aerial to achieve the post development linewidth. Where the resist samples the image is driven by the integrated development rate across the dose contours of the latent image and the gradient across those contours[41,42]. The coupling of the resist and the aerial image quality to achieve the final linewidth is also a factor of substrate reflections[43], resist absorbance, as well as chemical reactions at the substrate that poison the chemical reaction within the resist. In general, reflections degrade the latent image through the formation of standing waves. To develop through standing wave nodes the resist must be overexposed in the anti-nodal regions. This overexposure acts to lower the contrast of the latent image formed in the resist during exposure. Absorbance in the resist needs to be balanced with the substrate reflection and the resist thickness to maximize the contrast of the latent image[44,45,46]. Likewise, if the resist is poisoned at the substrate it needs more relative exposure to clear the image, thus overexposing the remainder of the film[47]. These issues are true for any imaging case but are even more critical when trying to attain extreme resolution.

Since image CD dependence on focus is different depending on where the aerial image is sampled it becomes important for doing accurate and robust OPC to determine what NILS and intensity the resist samples to form the final image in the substrate. For dense lines, this can be done by measuring the isofocal region bias relative to the conjugate point for the set of defocused aerial images, adding that to the target CD to get an estimate of the image CD that gave rise to the final CD[42]. Then at this CD determine the NILS and the intensity threshold[48].

There are other issues with resists that must always be considered. The resist has to form a good etch or implant mask for pattern transfer. Further the resist must not exhibit pattern collapse[49], nor line edge roughness (LER) [50,51]. This latter problem is very serious for imaging below the 130 nm node because the LER may consume a significant amount of allowed variance in resist image size. This adds another component to resist process selection that researchers at IBM recently addressed by using interferometric lithography to do LER screening of many resists[52]. This work showed at what image contrast LER started and its magnitude for many resists thus confirming what we proposed the first time this paper was published[3], that LER arises from the loss of NILS and insufficient exposure to adequately and uniformly modify the resist. In either case, PSM may delay its inevitable occurrence.

Other critical issues specific to resists deal with printing side-lobes that form in the resist when using attPSM and applying enough resist bias to sample the best processing region of the set of features and pitches being imaged. The resist solutions to these two desires are not only different but in many cases are in opposition to each other. It is these different responses that gives rise to the design methodology used in DELPHI. It is this method of image process integration that has been expanded from the case above to altPSM and binary masks.

Side-lobes are less likely to print when the resist has a highly non-linear development response to exposure. Because of their increased insensitivity to sub-E_0, formulations that do this tend to have small resist bias. A small bias is good for printing 1:1 lines and spaces and contact holes but is not good for printing lines with duty cycles greater than 1:1, for example 1:2. As shown in Figure 14, this small resist bias is not good for these larger pitch, small k_1 features because the point where the set of defocused images has the same image size, the conjugate point, is at the half-pitch and not at the feature size. The conjugate point gives rise to the isofocal region (IFR) in the resist, and slightly overexposed relative to it is the optimum process window[41,42]. This means that the larger the pitch, the larger the resist bias that is needed to bring the area of least sensitivity to exposure and focus into the desired target sizing range. At the extreme, the conjugate point for isolated lines is in a continuum near the maximum intensity of the aerial images. This is not something that can be properly corrected with feature bias -- isolated is isolated. To improve performance the line must be tricked into acting like it is dense. One way to do this is to place dummy lines to either side at a pitch that will give the desired IFR, like 1:1. The down side is these lines will print if they are not trimmed out by a secondary exposure and may cause a design challenge if they are to stay. Another way to do this is to add scattering bars as shown in Figure 2. Comparing this figure to Figure 14 shows that the image size response to intensity and focus for the primary 175 nm feature to 80 nm scattering bar distance of 290 nm and spacing between scattering bars of 135 nm looks like a good match to the 1:2 175 nm features shown.

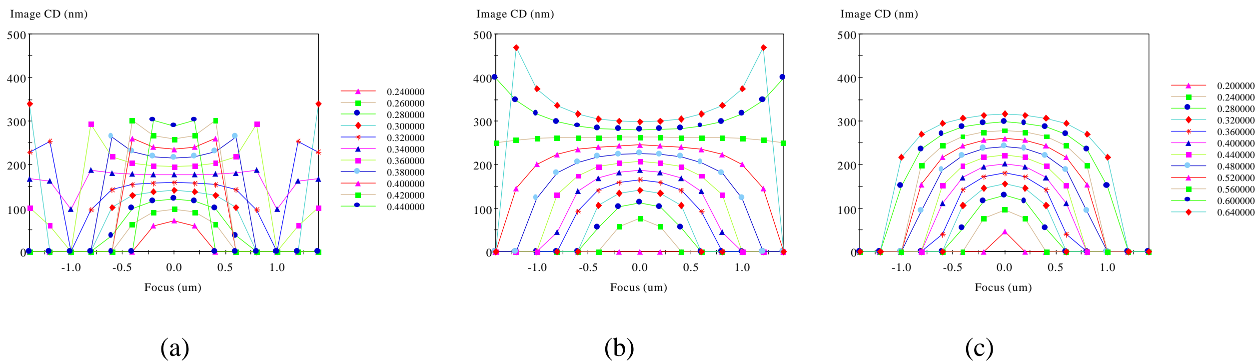

Figure 14: Aerial image size versus focus for different intensity thresholds for three different 175 nm feature duty cycles: (a) 1:1, (b) 1:2, and (c) 1:5. The conjugate is observed at the half pitch in the 1:1 and 1:2 features and is not present in any useable range in the 1:5 duty mask.

In general, it is a good idea to have minimal imaging bias using high contrast resists. In chemically amplified, positive acting photoresists the bias can be adjusted within limits with the post-exposure bake temperature[53] or novel thermal cycles created using multiple bakes[54]. After adjusting the resist bias in this way, the aerial image can be tuned with scattering bars to create a conjugate point if none exists and to match the intensity threshold to focus variation image size response. In this way the process window for the desired feature moves into the target range, without printing side-lobes and without hurting the image characteristics of other features. In this approach it is best to maximize the performance of the isolated line using binary scattering bars with or without weak phase shifting of the primary feature. Then the dense lines can be pulled into the common process window using OAI with or without weak PSM and biasing of the primary feature.

One factor whether phase shifting is used depends on how close in size the primary feature is to scattering bar size and how large the image process bias is. If the bias is sufficiently large it will sample the aerial image at an intensity threshold that is common to all features, not just the primary, so that they all print. Reducing process bias by raising the chemical contrast of the resist, or by raising the optical contrast with PSM, or to some degree with increasing primary mask bias, raises the image quality and reduces the process bias. Thus, reducing the image process bias causes the resist to sample the aerial image of the primary feature and not of the scattering bar. This is demonstrated in Figure 15. In this figure the aerial image for the mask is shown in the upper right corner for the mask in the upper left. The mask has phase shifted primary 160 nm lines with transmission ranging from 0% to 24% and a 800 nm space with dual 80 nm scattering bars inserted in the space between the primaries, spaced 240 nm from the primary. The aerial image for several different attPSM transmissions are shown and range from 0% to

42% in 6% increments. In this figure 36% to 42% has the best image quality, but as is shown even the 6% attPSM works.

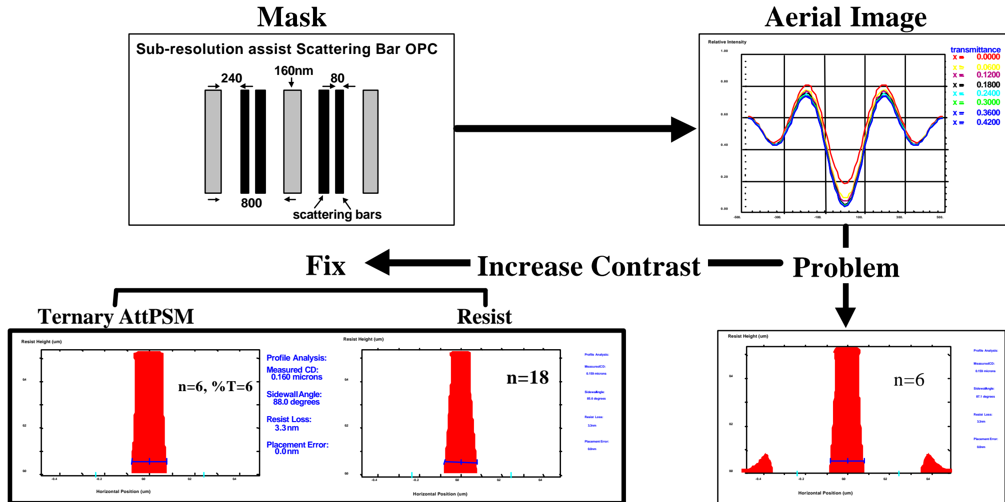

Figure 15: Sub-resolution assist features can print if not properly accounted for during process design. One way to eliminate the danger of printing is to raise the system contrast.

3. Experimental Example of Image Process Integration with Weak OAI

Let's briefly put image process integration to work. In this study, a process was designed for a 175 nm line on a 525 nm pitch and a 1050 nm pitch using a 0.53 NA, 248 nm stepper. The illuminator options were conventional, as well as strong and weak quads with center sigma of 0.6 and radial sigma of 0.25. These illuminators are shown in Figure 16. For a binary mask, the weak quad, relative to the strong, flattens the across pitch image CD size as well as the NILS for the two pitches of interest.

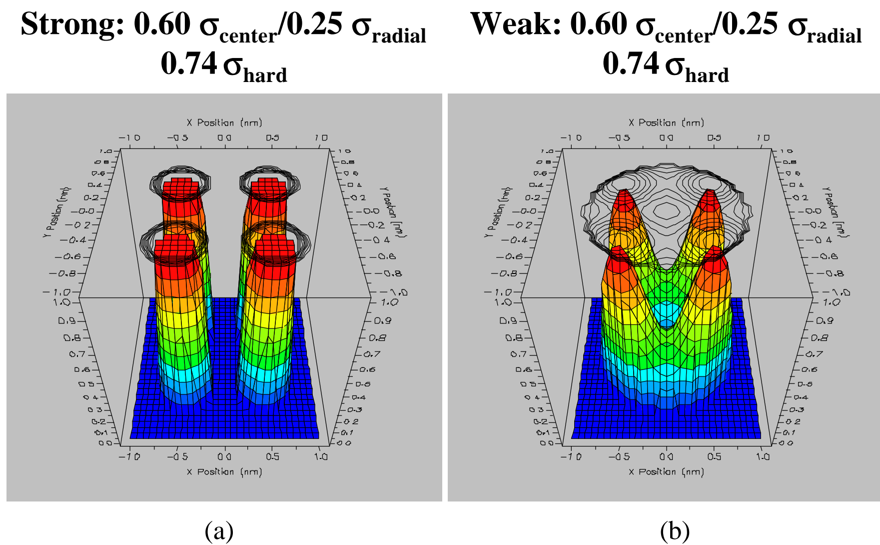

(a) (b)

Figure 16: Illumination source shapes used in the experimental work showing (a) strong (hard stop not shown), and (b) weak quadrupoles

Mask options were altPSM or binary masks, both without any OPC. As Figure 4 shows, altPSM has severe bias and while it could be made to work with OPC, the use of OAI with binary could accomplish the same thing and is simpler.

Shipley UV6, a resist with both good isolated line and dense line performance, was used for this work and coated on top of 60nm of Brewer Science AR2. By comparing the difference in size between the conjugate point and the isofocal region in the resist we estimate that the image process bias is 30 nm to 35 nm.

Figure 17 shows the experimentally obtained process windows for the 1:2 and 1:5 175 nm lines. These data show that, regardless of the illuminator, each feature has adequate latitude of its own, but that only the weak quad has any common process corridor. While the corridor is small, the use of a +10 to 20 nm bias for the dense lines should improve the situation. If more OPC is required, adding scattering bars as discussed for these features in section 2.3 would be the next step.

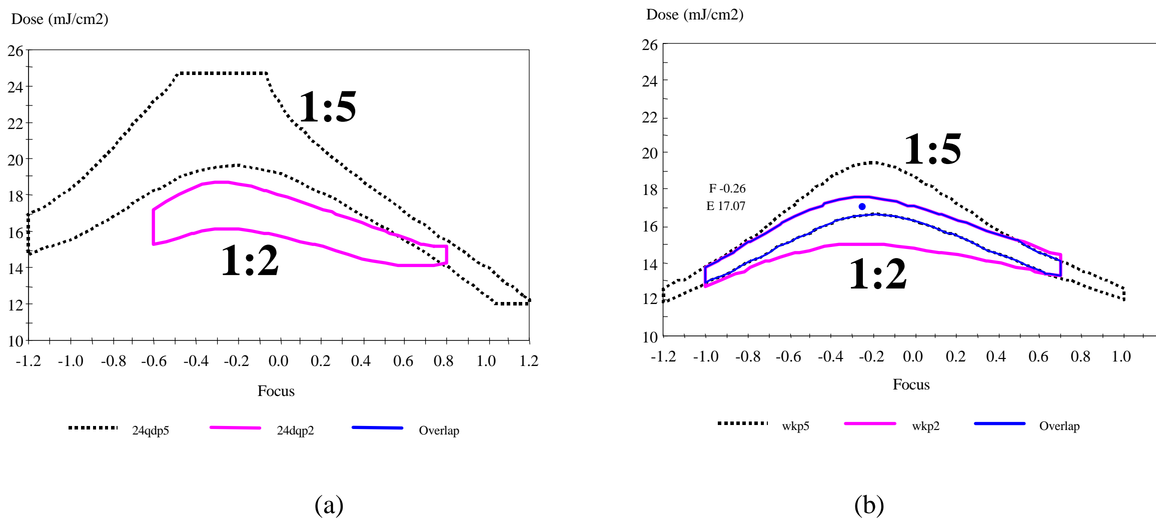

Figure 17: Experimental process windows (generated using ProDATA) for ±10% resist image size control for (a) strong quadrupole, and (b) weak quadrupole illuminators.

4. Achievable Resolution and the Hypothetical Roadmap

Based on our experimental and simulation work to date, plus a wealth of optical extension literature too numerous to site, Table I shows our predictions of the achievable resolution in production for isolated, dense and contact hole features. Each number is coded for the 130 nm (solid/underlined) 100 nm, (solid), and the 70 nm (gray) nodes. The crossed-out numbers represent conditions that will not be used. Wavelength is in columns and NA in rows. This table assumes 500 nm depth of focus with 5% exposure latitude over the entire focal depth; and in the 248 nm and the center 193 nm column 20% production resolution lost to aberrations. The final 193 nm column shows the improvement that can be gained by reducing the impact of aberration to 5%. This table shows for line features that 248 nm can be used all the way through the 130 nm SIA technology node and 193 nm can be used through the 100 nm node. Contacts, if the SIA sizing targets are real, will always be the most difficult level to do and is where the next generation of optics or otherwise would be inserted first, especially if 1:1 contacts are required.

Next is the hypothetical roadmap based on Table I with possibilities for setting up an imaging process from the 180 nm to the beginning of the 70 nm node. Hypothetically speaking, except possibly for contacts, the 130 nm technology node and its three shrinks can be done with 248 nm. At the beginning of the node lines can be imaged with altPSM, conventional illumination or with HTTattPSM, weak OAI and will finish using the former, at least for dense lines and does not preclude using a hybrid reticle with altPSM, for dense, and HTTattPSM for isolated. Contacts can be made with HTTattPSM, conventional illumination, but the pitch for the Bessel-type contact is

limited by wavelength/NA[27]. This needs further study to find ways to reliably image smaller pitches. The end of the node will require 193 nm for the contacts. Throughout this node thin single layer resist with an underlying hard mask will be required for producing quality pattern transfer masks.

Likewise, except for wavelength and resists, 193 nm replacing 248 nm, the 100 nm technology node and its shrinks can be done like the 130 nm node. The resists will be part of a thin layer imaging scheme such as bilayer. The end of the node may require a new optical technique like IIL, a new wavelength such as 157 nm, or a non-optical lithography.

To accomplish the goals set out in these tables we need to improve the process of image integration. This means starting at circuit design and layout to limit geometries so that there are no critical features at angles, using only Manhattan features; and then using strongly grid-based designs for easy scaling and OPC adjustment. Also, use designs that are altPSM friendly so that there are no phase conflicts and all critical features can be phase-shifted. For exposure we need tunable illuminators, aberration smart designs that are insensitive to the change in illumination and mask schemes and non-linear resists with threshold adjusts to eliminate the possibility of printing side-lobes. With respect to masks, we need HTTattPSM and altPSM blanks and zero bias fabrication techniques with overlay of less than 60 nm mask dimension for the different levels. Finally we need accurate SEM, phase and transmission metrology of live features, hierarchical inspection using the actinic wavelength and phase and transmission repair capability.

If all these things are accomplished, working together toward imaging process integration, the hypothetical roadmap may provide a route worth traveling.

Table of Hypothetically Attainable Feature Sizes **Reduced Aberrations**

λ		248			193			193 (Reduced Aberrations)		
Feature		iso	dense	CH	iso	dense	CH	iso	dense	CH
Duty Cycle		1:3	1:1	1:2	1:3	1:1	1:2	1:3	1:1	1:2
NA	0.53	70	140	187	55	109	146	48	96	127
	0.57	65	131	174	51	102	135	44	89	119
	0.60	62	124	165	48	97	129	42	84	113
	0.63	59	118	157	46	92	123	40	80	107
	0.68	55	109	146	43	85	114	37	75	99
	0.70	53	106	142	41	83	110	36	72	97
	0.80	47	93	124	36	72	97	32	63	84
factor		0.25	0.50	0.33	0.25	0.50	0.33	0.25	0.50	0.33
nPitch (Ideal)		0.5	0.5	1.0	0.5	0.5	1.0	0.5	0.5	1.0
nPitch (Full Field)		0.6	0.6	1.2	0.6	0.6	1.2	0.53	0.53	1.05

$$feature_size = \frac{pitch_{normalized_Full_Field} \cdot factor \cdot \lambda}{NA}; \; factor_from_experiment$$

Full Field assumes 20% loss of workable resolution due to aberrations!

Blue=130nm node **Black=100nm node** **Gray=70nm node**

Table I. Prediction of the minimum attainable features sizes with optical lithography.

SIA Year and Technology Generation	Year Feature	1999 180nm	2001 150nm	2003 130nm	2006 100nm	2009 70nm
SIA Solution	**Litho Option**	248/193nm	193nm	193nm/NGL	NGL	NGL
Iso	**Optical Option**	248nm	248nm	248nm	193nm	193nm
	1st mask/illum	COG/Conv	attPSM/Off-Axis	altPSM/Conv	altPSM/Conv	altPSM/Conv
	2nd mask/illum	COG/Off-Axis	altPSM/conv	attPSM/Off-Axis	attPSM/Off-Axis	
	Resist	SLR	SLR	SLR + Hard mask	SLR + Hard Mask	TLI
Dense	**Optical Option**	248nm	248nm	248nm	193nm	193nm
	1st mask/illum	COG/Conv	attPSM/Off-Axis	altPSM/Conv	altPSM/Conv	altPSM/Conv
	2nd mask/illum		altPSM/conv	attPSM/Off-Axis	attPSM/Off-Axis	
	Resist	SLR	SLR	SLR + Hard mask	SLR + Hard Mask	TLI
Contact	**Optical Option**	248nm	248nm	**248nm**	193nm	NGL
	1st mask/illum	COG/Conv	attPSM/Conv	attPSM/Conv	attPSM/Conv	NGL
	2nd mask/illum	COG/Off-Axis	attPSM/Off-Axis?	attPSM/Off-Axis?	attPSM/Off-Axis?	NGL
	Resist	SLR	SLR	SLR + Hard mask	TLI	TLI

0.7 NA needed for 130nm node & 2nd mask/illum option

Solutions Known **Work Required** **Hard Work Required**

Table II. Hypothetical optical lithography roadmap.

5. Acknowledgments

The authors would like to thank the rest of the DELPHI team: Kurt Wampler and Roger Caldwell of MicroUnity; Alex Naderi, Kent Nakagawa, Doug VanDenBroeke, and Catherine Baker of Photronics; Michael Reilly, Martha Rajaratnam, and Jim Thackeray of Shipley; John Biafore of ARCH Chemical; Patrick Reynolds of Benchmark Technologies, Peter Zandbergen, a Philips assignee to International SEMATECH; and Michael Cangemi and Lena Zavyalova of Rochester Institute of Technology. We would also like to thank Karen Brown and Gene Feit for support of this project at International SEMATECH, as well as the entire organization. Finally, for his original support and involvement in DELPHI, we dedicate this work to the memory of Jim Dey.

References

[1] Semiconductor Industry Association, The National Technology Roadmap for Semiconductors Technology Needs, 1997 Edition (1997).
[2] A. Wong, T. Farrell, R. Ferguson, G. Lu, S. Mansfield, A. Molless, M. Neisser, R. Nunes, D. Samuels, A. Thomas, JSAP and IEEE 1997 Symp. On VLSI Tech. Digest of Technical Papers, p. 127-128 (June 10-12, 1997, Kyoto, Japan).
[3] J. S. Petersen, M. McCallum, N. Kachwala, R. J. Socha, J. F. Chen, T. Laidig, B. W. Smith, R. Gordon, C A. Mack, Proc. SPIE Vol. 3546, p. 288-303 (1998).
[4] PROLITH/2 6.03, FINLE Technologies, Austin, TX was the primary lithography simulator used in our work.
[5] M. D. Levenson and N. S. Viswanathan, IEEE Transactions On Electron Devices ED-29, No. 12, p. 1828-1836 (1982).
[6] B. J. Lin, Solid State Tech Vol.35, No. 1, p.43-47, (Jan., 1992).
[7] T. Brunner, Optical Eng. Vol. 32, p. 2337-2343 (1993).
[8] H. Fukuda, T. Terasawa, S. Okazaki, J. Vac. Sci. Technol. B9(6), p. 3113-3116 (1991).

[9] T. Sandstroem, Proc. SPIE Vol. 3334, p. 590-596 (1998).
[10] M. Erdelyi, Z. Bor, G. Szabo, F. K. Tittel, Proc. SPIE Vol. 3334, p. 579-589 (1998).
[11] X. Chen, and S. R. Brueck, Proc. SPIE Vol. 3331, p. 214-224 (1998).
[12] J. Randall, A. Tritchkov, R. Jonckheere, P. Jaenen, K. Ronse, Proc. SPIE Vol. 3334, p. 124-130 (1998).
[13] K. Adam, R. Socha, M. Dusa and A. Neureuther, Proc. SPIE Vol. 3546, p. 642-650 (1998).
[14] Chen, J. F., Laidig, T. Wampler, K. E., Caldwell, R. F., Naderi, A. R.; Van De Brooke, D., Proc. SPIE Vol. 3236, p. 382-396 (1997).
[15] M. D. Pouty, A. R. Neureuther, Proc. SPIE Vol. 1088, p. 228-232 (1984).
[16] H. Kanai, K. Kawano, S. Tanaka, E. Shiobara, M. Aoki, I. Yoneda, S. Ito, Proc. SPIE Vol. 2793, p. 165-173 (1996).
[17] S. Tanaka, H. Nakamura, K. Kawano, S. Inoue, Proc. SPIE Vol. 2726, p. 473-484 (1996).
[18] R. A. Ferguson, A. K. Wong, T. A. Brunner, L. W. Liebmann, Proc. SPIE Vol. 2440, p. 349-360 (1995).
[19] J. S. Petersen, R. J. Socha, A. Naderi, C. Baker, S. Rizvi, D. VanDenBroeke, N. Kachwala, F. Chen, T. Laidig, K. E. Wampler, R. Caldwell, S. Takeuchi, Y. Yamada, T. Senoh, M. McCallum, Proc. SPIE Vol. 3412, p. 503-520 (1998).
[20] R. L. Gordon, C. A. Mack, J. S. Petersen, Proc. SPIE Vol. 3546, p. 606-616 (1998).
[21] J. S. Petersen, A. Williams, G. K. Rich, D. A. Miller, A. M. Martinez, Proc. SPIE Vol. 3096, p. 375-382 (1997).
[22] W. Swanson, J. S. Petersen, W. P. Mo, J. Heck, Proc. SPIE Vol. 3678, paper 101 (1999) (to be published)
[23] J. S. Petersen, JJAP Series 3, Proc. of 1989 Intern. Symp. On MicroProcess Conference, p. 151-155 (1989).
[24] K. Tounai and N. Aizaki, Proc. SPIE Vol. 2726, p. 82-87 (1996).
[25] F. M. Schellenberg, M. D. Levenson, P. J. Brock, Proc. SPIE Vol. 1604, p. 274-296 (1991).
[26] F. M. Schellenberg, M. D. Levenson, P. J. Brock, Proc. SPIE Vol. 1604, p. 274-296 (1992).
[27] R. Socha, J. S. Petersen, F. Chen, T. Laidig, K. E. Wampler, R. F. Caldwell, Proc. SPIE Vol. 3546, p. 617-641 (1998).
[28] R. J. Socha, X. Shi, K. Holman, M. Dusa, W. Conley, J. S. Petersen, F. Chen, T. Laidig, K. Wampler, R. Caldwell, M. C. Chu, C. Su, K. Huang, C. Chen, F. Wang, C. Le, C. Pierrat, B. Su, Proc. SPIE Vol. 3679, paper 04 (1999 to be published)
[29] Z. M. Ma; A. Andersson, Proc. SPIE Vol. 3334, p. 543-552 (1998).
[30] J. F. Chen, T. Laidig, K. E. Wampler, R. Caldwell, M. Dusa, C. Takemoto, A. Romano, Proc. of the Microlithography Seminar INTERFACE'97 (sponsored by Olin Microelectronic Materials) p. 181-201 (1997).
[31] Yasuzato, T., Ishida, S., Kasama, K., Proc. SPIE Vol. 2440, p. 804-815 (1995).
[32] M. Rajaratnam, D. Pai, J. Thackeray, D. Kang, G. Orsula, M. Reilly, Micro- Nano- Engineering Conference '98 Abstract Book, Leuven, Belgium, p. 47-48 (to be published).
[33] C. A. Mack, KTI Microlithography Seminar Interface '89, p. 209-215 (1989).
[34] D. L. Fehrs, H. B. Lovering, R. T. Scruton, KTI Microlithography Seminar Interface '89, p. 217-230 (1989).
[35] B. W. Smith, L. Zavyalova, J. S. Petersen, Proc. SPIE Vol. 3334, p. 384-394 (1998).
[36] W. N. Partlo, P. J. Tompkins, P.G. Dewa, P. F. Michaloski, Proc. SPIE Vol. 1927, p. 137-157 (1993).
[37] B. W. Smith, "Optics of Photolithography", Microlithography: Science and Technology, ED J. R. Sheats and B. W. Smith, Marcel Dekker, Inc.,New York, New York (1998), p. 240-241.
[38] P. Zandbergen, G. R. Amblard, M. McCallum, J. S. Petersen, B. W. Smith, L. Zavyalova, Proc. SPIE Vol. 3679, paper 29 (1999 to be published)
[39] N. Kachwala, J. S. Petersen, M. Cangemi, F. Chen, M. McCallum, Proc. SPIE Vol. 3679, paper 05 (1999 to be published)
[40] T. Ogawa, M. Uematsu, F. Uesawa, M. Kimura, Proc. SPIE Vol. 2440, p.772-783 (1995).
[41] J. S. Petersen, A. E. Kozlowski, Proc. SPIE Vol. 469, p.46-56 (1984).
[42] J. S. Petersen, Proc. SPIE Vol. 1088, p. 540-567 (1989).
[43] T. Brunner, Proc. SPIE Vol. 1466, p. 297-308 (1997).
[44] T. Ohfuji, O. Nalamasu, D. Stone, J. Vac. Sci. Technol. B11, p. 2714-2719 (1993).
[45] G. Thommes, V. Weber, J. Image Sci. 29 p. 112 (1985).
[46] W. Conley, R. Akkapeddi, J. Fahey, G. Hefferon, S. Holmes, G. Spinillo, J. Sturtevant, K. Welsh, Proc. SPIE, p. 2195 461-477 (1994).
[47] J. S. Petersen, T. H. Fedynnyshyn, J. Thackeray, K. R. Dean, J. L. Sturtevant, R. A. Caprio, G. K. Rich and D. Miller, Journal of Photopolymer Science and Technology, Vol. 8 No. 4, p. 571-598 (1995).
[48] J. S. Petersen and J. L. Sturtevant, "Practical Process Design for Microlithography", SPIE Short Course Notes, SPIE, Bellingham, WA (1997, 1998, 1999 and contained in the 1999 video release of the course)
[49] X. Chen, Z. Zhang, S. R. J. Brueck, R. A. Carpio, J. S. Petersen, Proc. SPIE Vol. 3048, p. 309-318 (1997).
[50] Q. Lin, A. D. Katnani, T. A. Brunner, C. Dewan, C. Fairchok, D. Latulipe, J. P. Simons, K. E. Petrillo, K. Babich, D. E. Seeger, M. Angelopoulos, R. Sooriyakumaran, G. M. Wallraff, D. C. Hofer, Proc. SPIE Vol. 3333, p. 278-288 (1998).
[51] S. C. Palmateer, S. G. Cann, J. E. Curtin, S. P. Doran, L. M. Eriksen, A. R. Forte, R. R. Kunz, T. M. Lyszczarz, M. B. Stern, C. M. Nelson, Proc. SPIE Vol. 3333, p. 634-642, (1998).
[52] M. I. Sanchez, W. D. Hinsberg, F. A. Houle, J. A Hoffnagle, M. D. Morrison, Proc. SPIE Vol. 3678, paper 18 (1999 to be published).
[53] J. S. Petersen, J. D. Byers, Proc. SPIE Vol. 2724, p. 163-172 (1996).
[54] J. S. Petersen, J. D. Byers, R. A. Carpio, Microelectronic Engineering Vol. 35, p. 169-174 (1997).